

Radiative p_{\perp} -broadening of fast partons in an expanding quark-gluon plasma

B.G. Zakharov¹

¹*L.D. Landau Institute for Theoretical Physics, GSP-1, 117940, Kosygina Str. 2, 117334 Moscow, Russia*
(Dated: May 24, 2022)

We study contribution of radiative processes to p_{\perp} -broadening of fast partons in an expanding quark-gluon plasma. It is shown that the radiative correction to $\langle p_{\perp}^2 \rangle$ for the QGP produced in AA -collisions at RHIC and LHC may be negative, and comparable in absolute value with the non-radiative contribution. We have found that the QGP expansion enhances the radiative suppression of p_{\perp} -broadening as compared to the static medium.

PACS numbers:

I. INTRODUCTION

One of the major signals of the quark-gluon plasma (QGP) formation in heavy ion collisions at RHIC and LHC is the strong suppression of particle spectra at high transverse momenta. It is believed that this effect (usually called the jet quenching) is a consequence of parton energy loss in the QGP, which softens the jet fragmentation functions. The parton energy loss is dominated by the radiative mechanism through induced gluon emission [1–7]. The induced gluon emission is caused by multiple scattering of fast partons in the QGP. The induced gluon spectrum can be expressed via the Green function of a 2D Schrödinger equation with an imaginary potential [2, 4], which is proportional to the product $n\sigma_{q\bar{q}}(\rho)$, where n is the QGP number density and $\sigma_{q\bar{q}}(\rho)$ is the dipole cross section of scattering of a $q\bar{q}$ pair off the QGP constituent (here, ρ is the size of the $q\bar{q}$ -pair). In the quadratic approximation $\sigma_{q\bar{q}}(\rho) \approx C\rho^2$, the Hamiltonian of the Schrödinger equation takes the oscillator form with a complex frequency. The square of the frequency is proportional to the transport coefficient \hat{q} [2, 3] defined by the relation $\hat{q} = 2Cn$.

Besides the modification of the longitudinal jet structure due to the parton energy loss, multiple parton scattering in the QGP can also modify the transverse structure of the jet. For a single fast parton the mean squared transverse momentum (relative to its initial velocity) in a uniform medium is given by [3]

$$\langle p_{\perp}^2 \rangle = \hat{q}L, \quad (1)$$

where L is the path length in the medium. One could expect that the p_{\perp} -broadening of the leading parton in the jet should lead to an increase of azimuthal jet decorrelation in the di-jet events (or in decorrelation of a photon and the jet in the photon-jet events) in AA -collisions [8]. For a better understanding of the in-medium jet evolution, it would be interesting to compare the values of \hat{q} extracted from the R_{AA} data with that obtained from the jet p_{\perp} -broadening. However, due to a considerable background from the azimuthal jet decorrelation in pp collisions related to the Sudakov formfactors [8], experimental detection of the jet p_{\perp} -broadening is a difficult problem. This background is especially large for LHC energies. However, even at RHIC in Au+Au collisions at $\sqrt{s} = 0.2$ TeV, where the effect of Sudakov formfactors are weaker, the STAR Collaboration has not detected a statistically significant effect of the jet deflection in the QGP [9]. The first data from ALICE [10] for Pb+Pb collisions at $\sqrt{s} = 5.02$ TeV also do not allow to draw a definite conclusion on the jet p_{\perp} -broadening. But the new preliminary ALICE results [11] indicate that the jet p_{\perp} distribution in 5.02 TeV Pb+Pb collisions may be somewhat narrower than that in pp collisions. The situation with detecting the jet p_{\perp} -broadening can become better after improving the accuracy of the data [12, 13].

On the theoretical side, it would be interesting to understand the role of the radiative contribution to p_{\perp} -broadening. The radiative correction to p_{\perp} -broadening can come from the real and virtual induced gluon emission [14–16]. It was expected that, due to smallness of the formation length for dominating soft gluon emission, this effect can be viewed as a local renormalization of \hat{q} . In [15], within the oscillator approximation in the soft gluon limit, it was found that the radiative contribution to the mean p_{\perp}^2 , $\langle p_{\perp}^2 \rangle_r$, in a homogeneous QGP has a double logarithmic form

$$\langle p_{\perp}^2 \rangle_r \sim \frac{\alpha_s N_c \hat{q} L}{\pi} \ln^2(L/l_0), \quad (2)$$

where l_0 is the size on the order of the Debye radius in the QGP. For central AA -collisions ($L \sim 5$ fm) the radiative contribution to $\langle p_{\perp}^2 \rangle$ turns out to be comparable with that from ordinary multiple scattering [15]. In [15] the authors used the light-cone path integral (LCPI) formalism developed in [4]. The case of the transverse spectra has been addressed within the LCPI technique in our earlier work [17] (see also [5, 18]). In the formulation of [17], for $a \rightarrow bc$ transition the distribution of the particle b in the Feynman variable x and the transverse momentum is described by the diagram of Fig. 1a. The contribution from the virtual process $a \rightarrow bc \rightarrow a$ to the distribution of the final particle

a is described by the diagram of Fig. 1b. In the case of $a = b$ both the diagrams contribute to the radiative correction to p_{\perp} -broadening. The parallel lines for two-body parts in Fig. 1 correspond to the Glauber factors, that describe the initial and final state interaction for real and virtual processes, and the three-body part describes dynamics of the transverse motion of the $bc\bar{a}$ -state. The analytical expressions for the diagrams of Fig. 1 will be discussed below. Calculations of [15] correspond to the diagrams of Fig. 1, but the authors have not accounted for the effect of the Glauber factors for the initial and final states. In [19, 20] (as in [15] for a static medium), we have addressed the radiative correction to p_{\perp} -broadening with an accurate treatment of the Glauber factors. It was found that the effect of the final state Glauber factors on $\langle p_{\perp}^2 \rangle_r$ vanishes for the sum of the real and virtual diagrams. However, the initial state Glauber factors give a considerable negative contribution to $\langle p_{\perp}^2 \rangle_r$, and its absolute magnitude turns out to be bigger than the positive contribution from the diagrams of Fig. 1 evaluated without the Glauber factors. As a result, the radiative contribution to the mean p_{\perp}^2 turns out to be negative, and comparable to the ordinary non-radiative mean p_{\perp}^2 given by (1) (below we denote it by $\langle p_{\perp}^2 \rangle_0$). If this really occurs, then the absence of a signal of the jet deflection in the data [9, 10] may be due to a considerable compensation between the radiative and non-radiative contributions to p_{\perp} -broadening. To understand better whether or not this scenario is possible it is highly desirable to study the radiative p_{\perp} -broadening for a more realistic model with an expanding QGP. This is the purpose of the present paper. The case of the expanding QGP has been addressed previously in [21]. But there the effect of the Glauber factors has not been accounted for.

For an expanding QGP the transport coefficient decreases with the proper time τ . In the Bjorken model [22] without the transverse expansion $\hat{q}(\tau) = \hat{q}(\tau_0)(\tau_0/\tau)$ [23], where τ_0 is the QGP formation time. In this case, in the oscillator approximation, the induced gluon spectrum can be expressed through the Green function for the oscillator frequency $\propto 1/\sqrt{\tau}$. The induced gluon emission in the oscillator approximation, in an expanding QGP has been addressed in [24]. There it was shown that for the transport coefficient $\hat{q}(\tau) = \hat{q}(\tau_0)(\tau_0/\tau)^\alpha$ the resulting total radiative energy loss coincides with that for a static medium with an effective transport coefficient given by

$$\hat{q}_{st} = \frac{2}{L^2} \int_{\tau_0}^L d\tau \tau \hat{q}(\tau) \approx \frac{2}{2-\alpha} \hat{q}(L). \quad (3)$$

In [25] it was demonstrated by numerical calculations that for $\alpha \sim 0 - 1.5$ this scaling law works very well for the induced gluon spectrum as well. This means that for decreasing with τ $\hat{q}(\tau)$ the reduction of the radiation rate in the region of large τ , where $\hat{q}(\tau) < \hat{q}_{st}$, is almost compensated by its excess from the region of small τ , where $\hat{q}(\tau) > \hat{q}_{st}$. Of course, this scaling law is not valid for the non-radiative contribution to the mean p_{\perp}^2 , which for an expanding medium reads

$$\langle p_{\perp}^2 \rangle_0 = \int_0^L d\tau \hat{q}(\tau). \quad (4)$$

One could expect that it does not hold for the radiative contribution $\langle p_{\perp}^2 \rangle_r$ as well. Because there is no reason for the delicate compensation between the regions of large and small τ , even if it occurs for the gluon spectrum. However, from the point of view of the jet p_{\perp} -broadening the most interesting quantity is the ratio $\langle p_{\perp}^2 \rangle_r / \langle p_{\perp}^2 \rangle_0$, (which characterizes the relative effect of the radiative correction). For this ratio the violation of the dynamical scaling potentially could be smaller than that for $\langle p_{\perp}^2 \rangle_r$ and $\langle p_{\perp}^2 \rangle_0$ separately. Intuitively, one can expect that for the expanding scenario the ratio $\langle p_{\perp}^2 \rangle_r / \langle p_{\perp}^2 \rangle_0$ should be negative and bigger, in absolute value, than that for the static case. Because, the effect of the negative contribution from the initial parton rescatterings (which is mostly sensitive to the region of small τ) should be more pronounced for the decreasing $\hat{q}(\tau)$. Our numerical calculations confirm this.

The paper is organized as follows. In Section 2, we discuss the method for evaluation of the radiative contribution to the mean p_{\perp}^2 within the LCPI approach. In Section 3, we present the results of numerical calculations. Conclusions are contained in Section 4. In appendix, we give formulas necessary for numerical calculations of $\langle p_{\perp}^2 \rangle_r$ in the oscillator approximation.

II. THEORETICAL FRAMEWORK FOR EVALUATION OF p_{\perp} -BROADENING IN LCPI APPROACH

We will consider p_{\perp} -broadening for a fast quark, when the real process is $q \rightarrow qg$ splitting (i.e., $a = b = q$ and $c = g$), and the virtual one is $q \rightarrow qg \rightarrow q$. We assume that the initial quark with energy E is produced at $z = 0$ (we choose the z -axis along the initial quark momentum) in the QGP of thickness L . The radiative correction to the distribution of the final quark in x and p_{\perp} from the real process $q \rightarrow qg$ is described by the diagram of the type shown in Fig. 1a. And the virtual contribution is described by the diagram of the type of shown in Fig. 1b. If one disregards the collisional parton energy loss, the total energy of the two-parton state and the energy of the one-parton state are identical at $z \rightarrow \infty$. However, the medium changes the relative weight of the one-parton and two-parton states, and

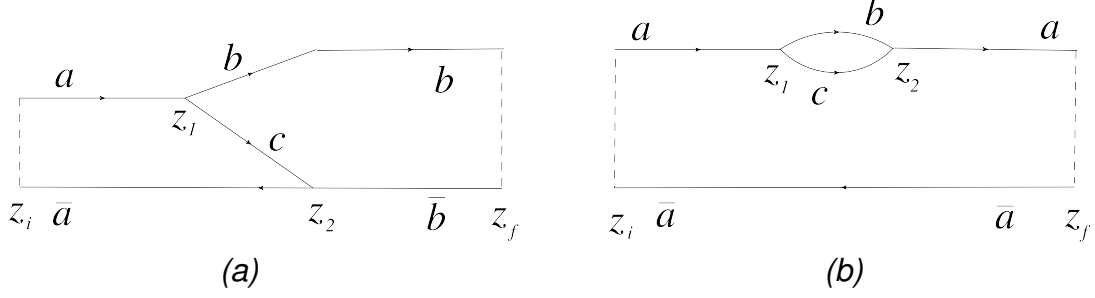


FIG. 1: (a) Diagram representation for the spectrum of the particle b for the $a \rightarrow bc$ process. (b) Diagram representation for the radiative correction to the spectrum of the particle a from the virtual process $a \rightarrow bc \rightarrow a$. There are also similar diagrams with transposition of vertices between the upper and lower parts of diagrams (a) and (b).

their transverse momentum distributions. As in [15], we consider the medium effect on the transverse momentum distribution for the final quark, which is integrated over its energy. For the virtual contribution the energy remains unchanged, but rescatterings in the medium of the intermediate two-particle state differ from rescatterings of a single quark. The radiative contribution to the mean quark p_{\perp}^2 due to the real and virtual process, associated with the interaction with the medium can be written as [15]

$$\langle p_{\perp}^2 \rangle_r = \int dx d\mathbf{p}_{\perp} \mathbf{p}_{\perp}^2 \left[\frac{dP}{dx d\mathbf{p}_{\perp}} + \frac{d\tilde{P}}{dx d\mathbf{p}_{\perp}} \right]_{ind}, \quad (5)$$

where $\frac{dP}{dx d\mathbf{p}_{\perp}}$ is the distribution in the Feynman variable $x = x_q$ and the transverse momentum of the quark for real process $q \rightarrow qq$, and $\frac{d\tilde{P}}{dx d\mathbf{p}_{\perp}}$ is the distribution for the virtual process $q \rightarrow qq \rightarrow q$. The subscript “ind” indicates that the purely vacuum contribution is subtracted. For the virtual process, x is determined by the Feynman variable of the quark in the intermediate qq state. The variable p_{\perp} in (5) for the real and virtual terms corresponds to the final quarks. Of course, formula (5) can be written in terms of the Feynman variable for the gluon, $x_g = E_g/E$, which is connected with x_q by the relation $x_q + x_g = 1$.

Let us consider first the real splitting. For $a \rightarrow bc$ splitting the distribution on the transverse momentum and the longitudinal fractional momentum of the particle b (which includes both the vacuum and the induced contributions) can be written in the form [17] (see also [20])

$$\frac{dP}{dx_b d\mathbf{p}_{\perp}} = \frac{1}{(2\pi)^2} \int d\tau_f \exp(-i\mathbf{p}_{\perp} \tau_f) F(\tau_f), \quad (6)$$

where

$$F(\tau_f) = 2\text{Re} \int_0^{\infty} dz_1 \int_{z_1}^{\infty} dz_2 \Phi_f(\tau_f, z_2) \hat{g} \mathcal{K}(\rho_2, z_2 | \rho_1, z_1) \Phi_i(\tau_i, z_1) \Big|_{\rho_2 = \tau_f, \rho_1 = 0}, \quad (7)$$

$$\Phi_i(\tau_i, z_1) = \exp \left[-\frac{\sigma_{a\bar{a}}(\tau_i)}{2} \int_0^{z_1} dz n(z) \right], \quad (8)$$

$$\Phi_f(\tau_f, z_2) = \exp \left[-\frac{\sigma_{b\bar{b}}(\tau_f)}{2} \int_{z_2}^{\infty} dz n(z) \right], \quad (9)$$

$\tau_i = x_b \tau_f$, $n(z)$ is the number density of the medium, $\sigma_{a\bar{a}}$ and $\sigma_{b\bar{b}}$ are the dipole cross sections for the $a\bar{a}$ and $b\bar{b}$ pairs, \hat{g} is the vertex operator, \mathcal{K} is the Green function for the Hamiltonian

$$H = \frac{\mathbf{q}^2 + \epsilon^2}{2M} - \frac{in(z)\sigma_{\bar{a}bc}(\tau_i, \rho)}{2}, \quad (10)$$

where $\mathbf{q} = -i\partial/\partial\rho$, $M = E_a x_b x_c$, $\epsilon^2 = m_b^2 x_c + m_c^2 x_b - m_a^2 x_b x_c$ with $x_c = 1 - x_b$, and $\sigma_{\bar{a}bc}$ is the cross section for the three-body $\bar{a}bc$ system. The relative transverse parton coordinates for the $\bar{a}bc$ state are given by $\rho_b - \rho_{\bar{a}} = \tau_i + x_c \rho$, $\rho_c - \rho_{\bar{a}} = \tau_i - x_b \rho$. The vertex operator in (7) reads

$$\hat{g} = \frac{P_a^b(x_b)g(z_1)g(z_2)}{8\pi M^2} \frac{\partial}{\partial \rho_1} \frac{\partial}{\partial \rho_2}, \quad (11)$$

where $P_a^b(x_b)$ is the standard $a \rightarrow b$ splitting function. Differentiation with respect to ρ_1 and ρ_2 on the right-hand side of (7) should be performed at a fixed τ_i , i.e. for a fixed position of the center mass of the bc pair. The Glauber factors Φ_i and Φ_f in (7) correspond to the parallel lines in Fig. 1 for the initial ($z < z_1$) and final ($z > z_2$) particles, and the Green function \mathcal{K} describes evolution of the three-body system in Fig. 1 between z_1 and z_2 . The factor 2 in (3) accounts for the contribution from the diagram that can be obtained by inter-exchange of the vertices between the upper and lower lines in Fig. 1.

For $q \rightarrow qg$ splitting the three-body cross section reads [26]

$$\sigma_{q\bar{q}g} = \frac{9}{8} [\sigma_{q\bar{q}}(\rho_{qg}) + \sigma_{q\bar{q}}(\rho_{g\bar{q}})] - \frac{1}{8} \sigma_{q\bar{q}}(\rho_{q\bar{q}}), \quad (12)$$

where

$$\sigma_{q\bar{q}}(\rho) = C_F C_T \int d\mathbf{q} \alpha_s^2(q^2) \frac{[1 - \exp(i\mathbf{q}\rho)]}{(q^2 + m_D^2)^2} = \frac{2}{\pi} \int d\mathbf{q} [1 - \exp(i\mathbf{q}\rho)] \frac{d\sigma}{dq^2}, \quad (13)$$

is the dipole cross section for the $q\bar{q}$ system, m_D is the Debye mass, C_F and C_T are the color Casimir operators for quark and the QGP constituent, $d\sigma/dq^2$ is the differential cross section for quark scattering off the QGP constituent. The ratio $C(\rho) = \sigma_{q\bar{q}}(\rho)/\rho^2$ is a smooth function of ρ . For the quadratic approximation

$$\sigma_{q\bar{q}}(\rho) = C\rho^2, \quad C = \hat{q}C_F/2C_{An}, \quad (14)$$

the Hamiltonian (10) can be written in the oscillator form. For an expanding medium the oscillator frequency depends on z .

The purely vacuum contribution to $a \rightarrow bc$ splitting in (7) comes from the region of large $z_{1,2}$ up to $z_f = \infty$. For an accurate treatment of the contribution of this region, an adiabatically switching off coupling should be used in the vertex factor (11). To separate the vacuum contribution it is convenient to write the product $\Phi_f \hat{g} \mathcal{K} \Phi_i$ on the right-hand side of (7) as (we omit arguments for clarity)

$$\Phi_f \hat{g} \mathcal{K} \Phi_i = \Phi_f \hat{g} (\mathcal{K} - \mathcal{K}_v) \Phi_i + (\Phi_f - 1) \hat{g} \mathcal{K}_v \Phi_i + \hat{g} \mathcal{K}_v (\Phi_i - 1) + \hat{g} \mathcal{K}_v. \quad (15)$$

Here \mathcal{K}_v is the vacuum Green function, and the last term on the right-hand side of (15) corresponds to the ordinary vacuum splitting. Its contribution can be calculated using the adiabatically switching off coupling $g(z) = g \exp(-\delta z)$ and taking the limit $\delta \rightarrow 0$ (see [20] for details). This leads to the vacuum spectrum

$$\frac{dP_v}{dx d\mathbf{p}_\perp} = \frac{\alpha_s P_{ba}(x)}{2\pi^2} \frac{\mathbf{p}_\perp^2}{(\mathbf{p}_\perp^2 + \epsilon^2)^2}, \quad (16)$$

where P_{ba} is the conventional $a \rightarrow b$ splitting function. Note that calculation of the medium dependent contribution to the spectrum of the last but one term in (15) also requires using the adiabatically switching off coupling. The region of very large $z_{1,2}$ is not important for the first two terms on the right hand side of (15), and they can be calculated with a z -independent coupling.

The distribution $\frac{d\tilde{P}}{dx d\mathbf{p}_\perp}$ for the virtual process $a \rightarrow bc \rightarrow a$, which is described by the diagram of Fig. 1b, can be written in the form similar to that for the real process by replacing F by its virtual counterpart \tilde{F} , given by

$$\tilde{F}(\tau_f) = -2\text{Re} \int_0^\infty dz_1 \int_{z_1}^\infty dz_2 \Phi_f(\tau_f, z_2) \hat{g} \tilde{\mathcal{K}}(\rho_2, z_2 | \rho_1, z_1) \Phi_i(\tau_i, z_1) \Big|_{\rho_2 = \rho_1 = 0}. \quad (17)$$

Except for the opposite sign, the functional form of \tilde{F} is similar to that for F , given by (7), but now we have $\tau_i = \tau_f$, and the Green function (we denote it $\tilde{\mathcal{K}}$), for the three-body part between z_1 and z_2 , should be calculated at $\rho_1 = \rho_2 = 0$. The change of the sign in (17) as compared to (7) occurs due to the fact that for the virtual process both the vertices, for parton splitting and merging, belong to the amplitude (upper part of the graph of Fig. 1b), which changes the sign of the vertex operator (11). Note that, similarly to the Green function \mathcal{K} entering the formula (7) for F , the Green function $\tilde{\mathcal{K}}$ in (17) has a hidden dependence on τ_f coming from the τ_f -dependence of its Hamiltonian. For $\tilde{\mathcal{K}}$ the Hamiltonian is also given by (10), but now with $\tau_i = \tau_f$. It is important that due to different relations between τ_i and τ_f for the real and virtual diagrams, the initial Glauber factors $\Phi_i(\tau_i)$ in (7) and (17) differ as well.

It is evident that $\langle p_{\perp}^2 \rangle_r$ can be expressed in terms of the Laplacian of function $F + \tilde{F}$ with respect to $\boldsymbol{\tau}_f$ at $\boldsymbol{\tau}_f = 0$ as¹

$$\langle p_{\perp}^2 \rangle_r = - \int dx [\nabla^2 F(\boldsymbol{\tau}_f) + \nabla^2 \tilde{F}(\boldsymbol{\tau}_f)] \Big|_{\boldsymbol{\tau}_f=0}. \quad (18)$$

We stress that calculation of the Laplacians in (18) should be performed treating the functions F and \tilde{F} as functions of $\boldsymbol{\tau}_f$ only, i.e., using the rigid connections $\boldsymbol{\rho}_2 = \boldsymbol{\tau}_f$, $\boldsymbol{\tau}_i = x\boldsymbol{\tau}_f$ for F and $\boldsymbol{\tau}_i = \boldsymbol{\tau}_f$ for \tilde{F} in calculating the initial Glauber factors Φ_i and the Green functions \mathcal{K} and $\tilde{\mathcal{K}}$. A simple calculation using the identity (15), after subtraction of the purely vacuum contributions, allows to represent $\langle p_{\perp}^2 \rangle_r$ as a sum of three terms

$$\langle p_{\perp}^2 \rangle_r = I_1 + I_2 + I_3, \quad (19)$$

where I_i are given by

$$I_1 = -2 \int dx \int_0^L dz_1 \int_0^{\infty} d\Delta z \text{Re} \left\{ \nabla^2 \hat{g} [\mathcal{K}(\boldsymbol{\rho}_2, z_2 | \boldsymbol{\rho}_1, z_1) - \mathcal{K}_v(\boldsymbol{\rho}_2, z_2 | \boldsymbol{\rho}_1, z_1)] \Big|_{\boldsymbol{\rho}_2=\boldsymbol{\tau}_f, \boldsymbol{\rho}_1=0, \boldsymbol{\tau}_f=0} \right. \\ \left. - \nabla^2 \hat{g} [\tilde{\mathcal{K}}(\boldsymbol{\rho}_2, z_2 | \boldsymbol{\rho}_1, z_1) - \tilde{\mathcal{K}}_v(\boldsymbol{\rho}_2, z_2 | \boldsymbol{\rho}_1, z_1)] \Big|_{\boldsymbol{\rho}_2=\boldsymbol{\rho}_1=0, \boldsymbol{\tau}_f=0} \right\}, \quad (20)$$

$$I_2 = -2 \int dx \int_0^L dz_1 \int_0^{\infty} d\Delta z \text{Re} \left\{ \hat{g} [\mathcal{K}(\boldsymbol{\rho}_2, z_2 | \boldsymbol{\rho}_1, z_1) - \mathcal{K}_v(\boldsymbol{\rho}_2, z_2 | \boldsymbol{\rho}_1, z_1)] \nabla^2 \Phi_i(x\boldsymbol{\tau}_f, z_1) \Big|_{\boldsymbol{\rho}_2=\boldsymbol{\tau}_f, \boldsymbol{\rho}_1=0, \boldsymbol{\tau}_f=0} \right. \\ \left. - \hat{g} [\tilde{\mathcal{K}}(\boldsymbol{\rho}_2, z_2 | \boldsymbol{\rho}_1, z_1) - \tilde{\mathcal{K}}_v(\boldsymbol{\rho}_2, z_2 | \boldsymbol{\rho}_1, z_1)] \nabla^2 \Phi_i(\boldsymbol{\tau}_f, z_1) \Big|_{\boldsymbol{\rho}_2=\boldsymbol{\rho}_1=0, \boldsymbol{\tau}_f=0} \right\} \\ = -2 \int dx f(x) \int_0^L dz_1 \langle p_{\perp}^2(z_1) \rangle_0 \int_0^{\infty} d\Delta z \text{Re} \hat{g} [\mathcal{K}(\boldsymbol{\rho}_2, z_2 | \boldsymbol{\rho}_1, z_1) - \mathcal{K}_v(\boldsymbol{\rho}_2, z_2 | \boldsymbol{\rho}_1, z_1)] \Big|_{\boldsymbol{\rho}_2=\boldsymbol{\rho}_1=0, \boldsymbol{\tau}_f=0}, \quad (21)$$

$$I_3 = \int dx \nabla^2 [\Phi_i(\boldsymbol{\tau}_f, L) - \Phi_i(x\boldsymbol{\tau}_f, L)] \Big|_{\boldsymbol{\tau}_f=0} \frac{dP_v}{dx} = -\langle p_{\perp}^2 \rangle_0 \int dx f(x) \frac{dP_v}{dx}, \quad (22)$$

Here $\langle p_{\perp}^2(z_1) \rangle_0 = \int_0^{z_1} \hat{q}(z) dz$, $f(x) = 1 - x^2$, $\Delta z = z_2 - z_1$, and dP_v/dx is the x -spectrum for vacuum given by

$$\frac{dP_v}{dx} = \int d\mathbf{p}_{\perp} \frac{dP_v}{dx d\mathbf{p}_{\perp}}. \quad (23)$$

In the expressions for $I_{2,3}$, we have used that

$$\hat{g} [\mathcal{K}(\boldsymbol{\rho}_2, z_2 | \boldsymbol{\rho}_1, z_1) - \mathcal{K}_v(\boldsymbol{\rho}_2, z_2 | \boldsymbol{\rho}_1, z_1)] \Big|_{\boldsymbol{\rho}_2=\boldsymbol{\tau}_f, \boldsymbol{\rho}_1=0, \boldsymbol{\tau}_f=0} = \hat{g} [\tilde{\mathcal{K}}(\boldsymbol{\rho}_2, z_2 | \boldsymbol{\rho}_1, z_1) - \tilde{\mathcal{K}}_v(\boldsymbol{\rho}_2, z_2 | \boldsymbol{\rho}_1, z_1)] \Big|_{\boldsymbol{\rho}_2=\boldsymbol{\rho}_1=0, \boldsymbol{\tau}_f=0}, \quad (24)$$

and the equalities

$$\nabla^2 \Phi_i(x\boldsymbol{\tau}_f, z_1) \Big|_{\boldsymbol{\tau}_f=0} = x^2 \nabla^2 \Phi_i(\boldsymbol{\tau}_f, z_1) \Big|_{\boldsymbol{\tau}_f=0}, \quad \nabla^2 \Phi_i(\boldsymbol{\tau}_f, z_1) \Big|_{\boldsymbol{\tau}_f=0} = -\langle p_{\perp}^2(z_1) \rangle_0. \quad (25)$$

The terms $I_{1,2}$ in (19) arise from calculating the Laplacian in $\boldsymbol{\tau}_f$ of the first term on the right hand side of (15), and I_3 of the third term. The second term on the right hand side of (15) does not contribute to $\langle p_{\perp}^2 \rangle_r$ because its Laplacian (for sum of the real and virtual terms) vanishes at $\boldsymbol{\tau}_f = 0$. The integral over p_{\perp} in (23) diverges logarithmically for large p_{\perp} . In numerical calculations, we regularized it by limiting the integration region to $p_{\perp} < p_{\perp}^{max}$ with

¹ We assume that the factors F and \tilde{F} are calculated in the quadratic approximation (14). The formula (18) should be valid to a logarithmic accuracy beyond the quadratic approximation as well, if $\boldsymbol{\tau}_f = 0$ is replaced by $\boldsymbol{\tau}_f \sim 1/p_{\perp}^{max}$.

$p_{\perp}^{max} = E \min(x, (1-x))$. We use expressions (19)–(22) for numerical calculations. The formulas required for calculating $I_{1,2}$ in the oscillator approximation are given in Appendix.

The integrand in the formula (20) for I_1 behaves as $1/\Delta z$ for $\Delta z \rightarrow 0$, which leads to the logarithmic divergence of I_1 . In the LCPI approach it is assumed that the typical $|z_2 - z_1|$ (i.e., the formation length L_f) is bigger than the correlation radius of the medium. For the QGP it is the Debye radius. For this reason, it is reasonable to regularize the integration over Δz taking the lower limit in (20) at $\Delta z \sim 1/m_D$. This prescription was used in [15] in calculating with a logarithmic accuracy the analogue of our contribution I_1 . As we mentioned in the Introduction, in [15] the Glauber factors $\Phi_{i,f}$ have not been accounted for. For this reason, the terms $I_{2,3}$ which contain $\nabla^2 \Phi_i$ have been missed. It will be seen from the numerical calculations that these terms give a negative contribution which is larger in magnitude than I_1 .

One remark should be made about the application of the above formulas to the p_{\perp} -broadening in the real QGP. Formally, in the oscillator approximation, one can use a unique transport coefficient for calculating the Green function and the Glauber factors. However, physically it is clear that the values of the transport coefficient that enters the Hamiltonian (via the oscillator frequency (A7)) and the Laplacian of the Glauber factor Φ_i (25) (via $\langle p_{\perp}^2 \rangle_0$) may differ due to the Coulomb effects. The transport coefficient of the fast quark (we will denote it \hat{q}' , and leave the notation \hat{q} for the transport coefficient that enters the oscillator frequency) that controls $\langle p_{\perp}^2 \rangle_0$ can be written in a simple probabilistic form [3, 23, 27]

$$\hat{q}' = n \int_0^{p_{\perp}^{max}} dp_{\perp}^2 p_{\perp}^2 \frac{d\sigma}{dp_{\perp}^2} \quad (26)$$

with $p_{\perp}^{max} \sim 3ET$, T the QGP temperature, $d\sigma/dp_{\perp}^2$ the differential cross section for quark scattering off the thermal parton. The transport coefficient for the Hamiltonian for the induced gluon emission it is reasonable to define as $\hat{q} = 2nC(\rho_{eff})$ [4, 28], where ρ_{eff} is the typical size of the gq -state. From the Schrödinger diffusion relation one obtains for soft gluons $\rho_{eff} \sim \sqrt{2L_f^{eff}/\omega}$. Here L_f^{eff} is the effective in-medium gluon formation length, which in the oscillator approximation is given by the inverse oscillator frequency $1/|\Omega|^2$. For the relevant region $\rho_{eff} \lesssim 1/m_D$, with the help of the double gluon formula (13), one can show that the product $2nC(\rho_{eff})$ coincides with (26) but with $p_{\perp}^{max} \sim 10/\rho_{eff}^2$ (see, e.g. [29]). This prescription gives the value of the transport coefficient \hat{q} about \hat{q}' calculated for the quark energy $\sim \omega$. For RHIC and LHC conditions, for gluon emission from a quark with $E \sim 30 - 100$ GeV the typical gluon energy $\bar{\omega} \sim 3 - 5$ GeV, i.e., $\bar{\omega}/E \ll 1$. Although, \hat{q}' has a smooth (logarithmic) dependence on E , the ratio $r = \hat{q}'/\hat{q}$ may differ significantly from unity due to the fact that $E \gg \bar{\omega}$. As will be seen below this gives a considerable effect on the magnitude of $\langle p_{\perp}^2 \rangle_r$.

Finally, we would like to make a remark on the physical interpretation of the I_3 term, which, as will be seen below, may dominate in the sum (19). From (22) one sees that I_3 contains $\langle p_{\perp}^2 \rangle_0$ for the whole medium, and the vacuum spectrum dP_v/dx without medium modification. At first glance, this says that the I_3 is connected with real and virtual gluon emission outside the medium from the initial parton which has undergone multiple scattering in the whole medium. However, this interpretation is completely wrong. In reality the vacuum like gluon emission occurs at the longitudinal distances which may be much smaller than the QGP size. Say, for jets with $E \lesssim 100$ GeV the typical z -scale for the vacuum like gluon emission is $\lesssim 1$ fm [30], and the typical jet path length in the QGP is ~ 5 fm. For this reason, it is clear that typically for the vacuum like gluon emission we have a situation with multiple scattering in the QGP of the final partons (say, if the QGP is formed at $\tau_0 \gtrsim 1$ fm, the contribution of the initial parton rescatterings will be very small). The form of the I_3 term is just a nontrivial consequence of the representation of the product $\Phi_f \hat{g} \mathcal{K} \Phi_i$ in the rearranged form on the right hand side of (15), and of the fact that the color charge of the final quark equals to that for the initial quark. But one should bear in mind that the decomposition on the right hand side of (15) by adding and subtracting the terms with the vacuum Green function is an artificial procedure, and only the full sum, given on the left hand side of (15), matters. For this reason, all the terms in (19) have the same status, and it does not make sense to say that the I_3 is connected with a specific mechanism due to rescatterings of the initial quark in the whole medium and its subsequent splitting into gq state outside the QGP. Of course, such processes are possible, but their contribution to p_{\perp} -broadening becomes very small at $L \gg 1$ fm.

² It can be easily obtained from the Schrödinger diffusion relation and the relation $\hat{q}_g \rho_{eff}^2 L_f^{eff}/4 \sim 1$ (which says that for the $gq\bar{q}$ system attenuation becomes strong at the longitudinal scale L_f^{eff}). Here we used the gluon transport coefficient, because for soft gluons $gq\bar{q}$ system interacts with the medium as a color singlet gq -pair.

TABLE I: The results for $m_q = 300$ MeV, $m_g = 400$ MeV obtained with $\hat{q}' = \hat{q}$ and with $\hat{q}' = r\hat{q}$ (the numbers in brackets)

	RHIC		LHC	
	expanding	static	expanding	static
$I_1/\langle p_\perp^2 \rangle_0$	0.382(0.188)	0.503(0.25)	0.738(0.318)	0.938(0.404)
$I_2/\langle p_\perp^2 \rangle_0$	-0.277	-0.212	-0.145	-0.113
$I_3/\langle p_\perp^2 \rangle_0$	-0.668	-0.668	-1.01	-1.01
$\langle p_\perp^2 \rangle_r / \langle p_\perp^2 \rangle_0$	-0.563(-0.757)	-0.378(-0.63)	-0.416(-0.836)	-0.184(-0.719)
$\langle p_\perp^2 \rangle_0$ [GeV ²]	3.9(7.96)	2.61(5.3)	5.1(11.85)	3.4(7.89)

TABLE II: The same as in Table I, but for $m_q = 150$ MeV, $m_g = 200$ MeV

	RHIC		LHC	
	expanding	static	expanding	static
$I_1/\langle p_\perp^2 \rangle_0$	0.468(0.231)	0.617(0.304)	0.815(0.351)	1.046(0.451)
$I_2/\langle p_\perp^2 \rangle_0$	-0.309	-0.237	-0.152	-0.118
$I_3/\langle p_\perp^2 \rangle_0$	-0.863	-0.863	-1.21	-1.21
$\langle p_\perp^2 \rangle_r / \langle p_\perp^2 \rangle_0$	-0.704(-0.941)	-0.483(-0.796)	-0.547(-1.011)	-0.282(-0.877)
$\langle p_\perp^2 \rangle_0$ [GeV ²]	3.9(7.96)	2.61(5.3)	5.1(11.85)	3.4(7.89)

III. NUMERICAL RESULTS

We will consider p_\perp -broadening for conditions of central heavy ion collisions at RHIC and LHC. We assume that the plasma fireball is produced at the proper time $\tau = 0.5$ fm. For the fast parton path length in the QGP we take $L = 5$ fm, which is the typical jet path length in the QGP for Au+Au(Pb+Pb) collisions at RHIC(LHC). We neglect the variation of the initial QGP temperature in the impact parameter. In this case, z -dependence of the transport coefficient along the fast parton path coincide with its τ -dependence. We describe the QGP evolution at $\tau > \tau_0$ within Bjorken's model [22] without the transverse expansion that leads to the entropy density $s \propto 1/\tau$. Within the ideal gas model it gives $\hat{q}(z) = \hat{q}_0(\tau_0/z)$ at $z > \tau_0$, where \hat{q}_0 is the value of the transport coefficient at $\tau = \tau_0$. To account for qualitatively the fact that the QGP formation is not instantaneous we take $\hat{q}(z) = \hat{q}_0(z/\tau_0)$ for $z < \tau_0$.

For main variant we use the quasiparticle masses $m_q = 300$ MeV and $m_g = 400$ MeV, which were obtained within quasiparticle model from the lattice data in [31] for temperatures relevant for RHIC and LHC conditions. With these values of the quasiparticle masses, in [32, 33], we successfully described the RHIC and LHC data on the nuclear modification factor R_{AA} . To understand the uncertainties associated with the parton masses, we also perform calculations for masses $m_q = 150$ MeV and $m_g = 200$ MeV. As in [15], we take $\alpha_s = 1/3$ at the vertex of the $q \rightarrow qg$ transition. Also, like in [15], we regularize the $1/\Delta z$ divergence in (20) by truncating the integration at $\Delta z_{min} = 1/m$ with $m = 300$ MeV. In (20)–(22) we integrate over x from $x_{min} = m_q/E$ up to $x_{max} = 1 - m_g/E$ (recall that we define x as x_q ; in terms of x_g , our integration region corresponds to the variation of x_g from m_g/E to $1 - m_q/E$).

To fix the value of the parameter \hat{q}_0 in the above parametrization of $\hat{q}(z)$ we use the results of our previous analyses of jet quenching beyond the oscillator approximation. In [32, 33] we have performed calculations of R_{AA} with running α_s beyond the the oscillator approximation with accurate treatment of the Coulomb effects. To make our analysis as accurate as possible we adjusted the value of \hat{q}_0 to reproduce the quark energy loss ΔE for the running α_s in the model of [33] with the Debye mass from the lattice calculations [34]. This procedure gives $\hat{q}_0 \approx 0.551$ GeV³ at $E = 30$ GeV for Au+Au collisions at $\sqrt{s} = 0.2$ TeV and $\hat{q}_0 \approx 0.719$ GeV³ at $E = 100$ GeV for Pb+Pb collisions at $\sqrt{s} = 2.76$ TeV³ (we call these variants the RHIC(LHC) versions). In terms of the \hat{q}_{st} for the static scenario given by (3) our RHIC(LHC) versions correspond to $\hat{q}_{st} \approx 0.103(0.134)$ GeV³. We have used a similar running α_s and the Debye mass to determine the introduced in section 2 the coefficient r describing the enhancement of the transport coefficient entering the Glauber factor. We obtained for the RHIC(LHC) versions $r \approx 2(2.3)$. We are fully aware that the errors in the factor r may be rather large. But the fact that \hat{q}'/\hat{q} should be ~ 2 seems to be fairly reliable.

In Table I we present the results for the ratio of the terms $I_{1,2,3}$ and of the total $\langle p_\perp^2 \rangle_r$ to the $\langle p_\perp^2 \rangle_0$ for our main variant of the parton masses ($m_q = 300$ MeV and $m_g = 400$ MeV). We also give $\langle p_\perp^2 \rangle_0$. We present the results both

³ We use the transport coefficient of the quark which is smaller than the gluon transport coefficient by a factor of $C_F/C_A = 4/9$.

for the expanding and for static models. For the static case the calculations are performed using \hat{q}_{st} . The results for the set $m_q = 150$ MeV and $m_g = 200$ MeV are given in Table II. The comparison of the results from Tables I and II, shows that the sensitivity of the predictions to the parton masses turns out to be not very strong. Note that the sensitivity of the induced gluon emission to the mass of the light quark is generally low (except for the emission of hard gluons with $x_g \sim 1$), and the change in the predictions is mainly due to variation of m_g .

From Tables I and II, one can see that in all the cases $\langle p_\perp^2 \rangle_r < 0$. This occurs because the negative contribution from the $I_{2,3}$ terms turns out to be larger in magnitude than the positive contribution of the I_1 . Note that, as we expected, the relative effect of the negative contribution to the mean p_\perp^2 from the Glauber factors becomes bigger for the expanding QGP. The negative $\langle p_\perp^2 \rangle_r$ can lead to a sizable reduction of the total (non-radiative plus radiative) mean p_\perp^2 . For the version with $\hat{q}' = \hat{q}$ the reduction is approximately by half for the expanding scenario. For the version with $\hat{q}' > \hat{q}$ the magnitude of the negative radiative contribution is comparable to that from the non-radiative mechanism, and the total mean p_\perp^2 may be very small. However, one should bear in mind that this conclusion may depend on the value of the I_1 term, which requires the Δz -regularization. To understand the sensitivity of the results to the lower limit of the Δz -integration in (20), we have performed calculations for $\Delta z_{min} = 1/m$ with $m = 600$ MeV. In this case I_1 becomes bigger by a factor of $\sim 2.5(2)$ for RHIC(LHC). This gives $\langle p_\perp^2 \rangle_r / \langle p_\perp^2 \rangle_0 \approx 0.01(-0.47)$ for $\hat{q}'/\hat{q} = 1(r)$ for RHIC, and $\langle p_\perp^2 \rangle_r / \langle p_\perp^2 \rangle_0 \approx 0.37(-0.5)$ for $\hat{q}'/\hat{q} = 1(r)$ for LHC. Thus, we see that, for the clearly more realistic version with $\hat{q}' > \hat{q}$, the radiative correction to the mean p_\perp^2 is negative, and may suppress the mean p_\perp^2 by a factor of ~ 2 .

In the above, we presented results of the fixed coupling computations within the oscillator approximation for the dipole cross section. Accurate calculations of the $I_{1,2}$ terms for the running coupling and the double gluon $\sigma_{q\bar{q}}(\rho)$ (13) is a complicated problem. However, for the ratio $I_3/\langle p_\perp^2 \rangle_0$ the form of $\sigma_{q\bar{q}}(\rho)$ is unimportant, and the generalization to the running α_s can be easily done by replacing in dP_v/dx the fixed α_s by the running one [20]. We performed such calculations with the one-loop α_s frozen for small momenta at the value $\alpha_s^{fr} = 0.7$, which was obtained earlier from analysis of the low- x structure functions within the dipole BFKL equation [36]. This value is also supported by the analysis of heavy quark energy loss in vacuum [37]. For expanding scenario (and parton masses as in Table I), this procedure, while keeping $I_{1,2}/\langle p_\perp^2 \rangle_0$ unchanged, gives $\langle p_\perp^2 \rangle_r / \langle p_\perp^2 \rangle_0 \approx -0.76(-0.97)$ for $\hat{q}'/\hat{q} = 1(r)$ for RHIC, and $\langle p_\perp^2 \rangle_r / \langle p_\perp^2 \rangle_0 \approx -0.5(-0.92)$ for $\hat{q}'/\hat{q} = 1(r)$ for LHC. These numbers are for the Δz -regularization of I_1 with $m = 300$ MeV. For $m = 600$ MeV we obtained $\langle p_\perp^2 \rangle_r / \langle p_\perp^2 \rangle_0 \approx -0.19(-0.59)$ for $\hat{q}'/\hat{q} = 1(r)$ for RHIC, and $\langle p_\perp^2 \rangle_r / \langle p_\perp^2 \rangle_0 \approx 0.29(-0.58)$ for $\hat{q}'/\hat{q} = 1(r)$ for LHC. As one can see, for the running α_s , the effect of the initial state rescatterings becomes somewhat stronger. As far as the accurate predictions for $I_{1,2}/\langle p_\perp^2 \rangle_0$ are concerned, intuitively, one can expect that the accurate calculations should give smaller values of $I_{1,2}/\langle p_\perp^2 \rangle_0$ than obtained in the present analysis. Indeed, for the Green functions in the formulas (20) and (21) the typical size of the intermediate three-body state (in the sense of their path integral representations) should be, more or less, similar to that for the induced gluon emission. But we adjusted \hat{q} (i.e. $2nC(\rho_{eff})$) to reproduce the induced gluon emission energy loss obtained with the running coupling and accurate $\sigma_{q\bar{q}}(\rho)$. This means that the variation of the $I_{1,2}/\langle p_\perp^2 \rangle_0$ should be approximately similar to the variation of the ratio $C(\rho_{eff})/C(1/p_{\perp max})$ (because $\langle p_\perp^2 \rangle_0 \propto C(1/p_{\perp max})$). However, for the accurate $C(\rho)$ this ratio will be smaller than that in the oscillator approximation (see e.g. [38]). Note that this occurs even without the logarithmic growth of $C(\rho)$ at $\rho \rightarrow 0$. Thus, one can expect that the accurate calculations should give smaller $I_{1,2}/\langle p_\perp^2 \rangle_0$. As a results, the effect of the negative contribution from the I_3 term on the $\langle p_\perp^2 \rangle_r / \langle p_\perp^2 \rangle_0$ will be more pronounced.

IV. CONCLUSIONS

We have studied the radiative p_\perp -broadening of fast partons in an expanding QGP for conditions of central Au+Au(Pb+Pb) collisions at RHIC(LHC). The analysis has been performed within the LCPI formalism [4, 17] in the oscillator approximation, accounting for the initial state rescatterings. Similarly to the case of the static QGP, addressed in [19, 20], we have found that the radiative correction may be negative, i.e., it may lead to reduction of p_\perp -broadening. The negative contribution to $\langle p_\perp^2 \rangle_r$ comes mostly from the difference of the initial state Glauber factors for the real and virtual processes. This effect appears naturally beyond the soft gluon approximation. Formally, this phenomenon is due to rescatterings of the initial parton for the vacuum like gluon emission. However, we argue that this interpretation is wrong, and the effect is dominated by rescatterings of the final fast parton.

We have found that the QGP expansion leads to a sizeable increase of the effect of the initial state rescatterings, as compared to the static QGP. Our numerical results show that for the RHIC and LHC conditions, due to the negative $\langle p_\perp^2 \rangle_r$ the total (non-radiative plus radiative) mean p_\perp^2 may be quite small. In light of this, it is possible that the negative experimental searches for the jet rescatterings in the QGP [9–11] may be due to a considerable reduction of p_\perp -broadening by the radiative contribution.

Acknowledgments

I am grateful to Peter Jacobs for drawing my attention to a new measurement of the jet p_{\perp} -broadening by the ALICE Collaboration [11] and helpful communication about the ALICE analysis of the jet deflection. This work is supported by the Program 0033-2019-0005 of the Russian Ministry of Science and Higher Education.

Appendix A: Formulas necessary for calculating the factors I_i

In this appendix, we give formulas necessary for numerical calculations of the contributions I_i in (19) with the help of (20)–(22) in the oscillator approximation. For quadratic parameterization of the dipole cross section $\sigma_{q\bar{q}}(\rho) = C\rho^2$ (in terms of quark transport coefficient $C = \hat{q}/2n$), the three-body cross section $\sigma_{\bar{a}bc}$ can be written as

$$\sigma_{\bar{a}bc}(\boldsymbol{\rho}, \mathbf{R}) = C_{b\bar{a}}(\boldsymbol{\rho}_b - \boldsymbol{\rho}_{\bar{a}})^2 + C_{c\bar{a}}(\boldsymbol{\rho}_c - \boldsymbol{\rho}_{\bar{a}})^2 + C_{bc}(\boldsymbol{\rho}_b - \boldsymbol{\rho}_c)^2, \quad (\text{A1})$$

where, $\boldsymbol{\rho} = \boldsymbol{\rho}_b - \boldsymbol{\rho}_c$, $\mathbf{R} = x_c\boldsymbol{\rho}_b + x_b\boldsymbol{\rho}_c - \boldsymbol{\rho}_{\bar{a}}$, $\boldsymbol{\rho}_b - \boldsymbol{\rho}_{\bar{a}} = \mathbf{R} + x_c\boldsymbol{\rho}$, and $\boldsymbol{\rho}_c - \boldsymbol{\rho}_{\bar{a}} = \mathbf{R} - x_b\boldsymbol{\rho}$. For process $q \rightarrow qg$ ($a = b = q$, $c = g$)

$$C_{bc} = C_{c\bar{a}} = \frac{9C}{8}, \quad C_{b\bar{a}} = -\frac{C}{8}. \quad (\text{A2})$$

For diagrams in Fig. 1a, $\mathbf{R} = \boldsymbol{\tau}_i$. It is convenient to write $\sigma_{\bar{a}bc}$ as

$$\sigma_{\bar{a}bc}(\boldsymbol{\rho}, \mathbf{R}) = Cp\mathbf{R}^2 + C_3\mathbf{u}^2, \quad (\text{A3})$$

where $C_3 = C_{b\bar{a}}x_c^2 + C_{c\bar{a}}x_b^2 + C_{bc}$, $p = [C_{b\bar{a}}C_{c\bar{a}} + C_{b\bar{a}}C_{bc} + C_{c\bar{a}}C_{bc}]/CC_3$, and the new variable \mathbf{u} is given by

$$\mathbf{u} = \boldsymbol{\rho} + \boldsymbol{\tau}_i V \quad (\text{A4})$$

with $V = (x_c C_{b\bar{a}} - x_b C_{c\bar{a}})/C_3$. The Hamiltonian (10) can be written in terms of the variable \mathbf{u} in the form

$$H = H_{osc} - \frac{i\hat{q}(z)p\boldsymbol{\tau}_i^2}{4} + \frac{\epsilon^2}{2M}, \quad (\text{A5})$$

where $\hat{q}(z) = 2n(z)C$ is the local transport coefficient, and H_{osc} is the harmonic oscillator Hamiltonian

$$H_{osc} = -\frac{1}{2M} \left(\frac{\partial}{\partial \mathbf{u}} \right)^2 + \frac{M\Omega^2 \mathbf{u}^2}{2} \quad (\text{A6})$$

with the complex z -dependent frequency

$$\Omega = \sqrt{\frac{-i\hat{q}(z)C_3}{2CM}}. \quad (\text{A7})$$

The Green function \mathcal{K} for the Hamiltonian (A5) can be written as

$$\mathcal{K}(\boldsymbol{\rho}_2, z_2 | \boldsymbol{\rho}_1, z_1) = K_{osc}(\mathbf{u}_2, z_2 | \mathbf{u}_1, z_1) \exp \left[-\frac{p\boldsymbol{\tau}_i^2}{4} \int_{z_1}^{z_2} q(z) - \frac{i(z_2 - z_1)\epsilon^2}{2M} \right], \quad (\text{A8})$$

where K_{osc} is the Green function for the oscillator Hamiltonian (A6). In general, for arbitrary $\Omega(z)$ the oscillator Green function can be written in the form [24, 35]

$$K_{osc}(\mathbf{u}_2, z_2 | \mathbf{u}_1, z_1) = \frac{\gamma}{2\pi i} \exp [i(\alpha\mathbf{u}_2^2 + \beta\mathbf{u}_1^2 - \gamma\mathbf{u}_1 \cdot \mathbf{u}_2)]. \quad (\text{A9})$$

The numerical method for evaluation of α , β , and γ will be discussed below.

In our formulas (20)–(22), the differential operator \hat{g} (11) is acting on the Green function \mathcal{K} at fixed $\boldsymbol{\tau}_i$. Therefore, in \hat{g} , we can replace $\frac{\partial}{\partial \boldsymbol{\rho}_2} \cdot \frac{\partial}{\partial \boldsymbol{\rho}_1}$ by $\frac{\partial}{\partial \mathbf{u}_2} \cdot \frac{\partial}{\partial \mathbf{u}_1}$. Then, from (A9) one obtains

$$\frac{\partial}{\partial \boldsymbol{\rho}_2} \cdot \frac{\partial}{\partial \boldsymbol{\rho}_1} \mathcal{K}(\boldsymbol{\rho}_2, z_2 | \boldsymbol{\rho}_1, z_1) = -[2i\gamma + (2\alpha\mathbf{u}_2 - \gamma\mathbf{u}_1) \cdot (2\beta\mathbf{u}_1 - \gamma\mathbf{u}_2)] \mathcal{K}(\boldsymbol{\rho}_2, z_2 | \boldsymbol{\rho}_1, z_1). \quad (\text{A10})$$

For the diagram in Fig. 1a, $\rho_1 = 0$, $\rho_2 = \tau_f = \tau_i/x_b$, and

$$\mathbf{u}_{1,2} = \tau_f k_{1,2}, \quad k_1 = x_b V, \quad k_2 = 1 + x_b V. \quad (\text{A11})$$

Then from (11) we obtain

$$\hat{g}\mathcal{K}(\rho_2, z_2 | \rho_1, z_1) \Big|_{\rho_{1,2}=\tau_f=0} = - \left(\frac{\alpha_s P_{ba}}{2M^2} \right) \cdot \frac{\gamma^2}{\pi} \exp \left[- \frac{i(z_2 - z_1)\epsilon^2}{2M} \right]. \quad (\text{A12})$$

For calculating I_1 (20), we need the Laplacian in τ_f for $\tau_f = 0$ of $\hat{g}\mathcal{K}(\rho_2, z_2 | \rho_1, z_1)$ at $\rho_2 = \tau_f$ and $\rho_1 = 0$. A simple calculation gives

$$\nabla_{\tau_f}^2 \hat{g}\mathcal{K}(\rho_2, z_2 | \rho_1, z_1) \Big|_{\rho_2=\tau_f, \rho_1=0, \tau_f=0} = \left(\frac{\alpha_s P_{ba}}{2M^2} \right) \cdot \frac{2\gamma(2\gamma D - G)}{i\pi} \exp \left[- \frac{i(z_2 - z_1)\epsilon^2}{2M} \right], \quad (\text{A13})$$

where

$$D = \alpha k_2^2 + \beta k_1^2 - \gamma k_1 k_2 + \frac{i x_b p}{4} \int_{z_1}^{z_2} dz \hat{q}(z), \quad (\text{A14})$$

$$G = (2\alpha k_2 - \gamma k_1)(2\beta k_1 - \gamma k_2). \quad (\text{A15})$$

For the vacuum Green function, one just has to replace in formulas (A12) and (A13) the functions α , β , and γ by their vacuum analogues

$$\alpha_0 = \beta_0 = \gamma_0/2 = \frac{M}{2(z_2 - z_1)}. \quad (\text{A16})$$

and to set $\hat{q}(z) = 0$. In this case one obtains $D_0 = \alpha_0$, $G_0 = 0$.

The formula (A12) holds for the Green function $\tilde{\mathcal{K}}$ for the virtual diagram in Fig. 1b as well. In the virtual counterparts of the formulas (A14) and (A15) $\tilde{k}_{1,2} = V$, and in the last term on the right-hand side of (A14) the factor x_b is absent. For the virtual vacuum contribution $\tilde{D}_0 = \tilde{G}_0 = 0$.

Let us finally discuss evaluation of the functions α , β , and γ . For a harmonic oscillator with a z -independent frequency Ω

$$\alpha = \beta = \frac{M\Omega}{2 \tan(\Omega(z_2 - z_1))}, \quad \gamma = \frac{M\Omega}{\sin(\Omega(z_2 - z_1))}. \quad (\text{A17})$$

For numerical calculations in the case of z -dependent frequency $\Omega(z)$ we use the z -slicing method based on the recurrent relations [35]

$$\begin{aligned} \alpha(z_{n+1}, z_1) &= \alpha(z_{n+1}, z_n) - \frac{\gamma^2(z_{n+1}, z_n)}{4[\alpha(z_n, z_1) + \beta(z_{n+1}, z_n)]}, \\ \beta(z_{n+1}, z_1) &= \beta(z_n, z_1) - \frac{\gamma^2(z_n, z_1)}{4[\alpha(z_n, z_1) + \beta(z_{n+1}, z_n)]}, \\ \gamma(z_{n+1}, z_1) &= \frac{\gamma(z_n, z_1)\gamma(z_{n+1}, z_n)}{2[\alpha(z_n, z_1) + \beta(z_{n+1}, z_n)]}. \end{aligned} \quad (\text{A18})$$

These relation can be readily obtained using (A9) and the convolution formula for the Green functions

$$K(\rho_3, z_3 | \rho_1, z_1) = \int d\rho_2 K(\rho_3, z_3 | \rho_2, z_2) K(\rho_2, z_2 | \rho_1, z_1). \quad (\text{A19})$$

[1] M. Gyulassy and X.N. Wang, Nucl. Phys. B**420**, 583 (1994) [nucl-th/9306003].

[2] R. Baier, Y.L. Dokshitzer, A.H. Mueller, S. Peigné, and D. Schiff, Nucl. Phys. B**483**, 291 (1997) [hep-ph/9607355].

- [3] R. Baier, Y.L. Dokshitzer, A.H. Mueller, S. Peigné, and D. Schiff, Nucl. Phys. B**484**, 265 (1997) [hep-ph/9608322].
- [4] B.G. Zakharov, JETP Lett. **63**, 952 (1996) [hep-ph/9607440].
- [5] U.A. Wiedemann, Nucl. Phys. A**690**, 731 (2001) [hep-ph/0008241].
- [6] M. Gyulassy, P. Lévai, and I. Vitev, Nucl. Phys. B**594**, 371 (2001) [hep-ph/0006010].
- [7] P. Arnold, G.D. Moore, and L.G. Yaffe, JHEP **0206**, 030 (2002) [hep-ph/0204343].
- [8] A.H. Mueller, B. Wu, B.-W. Xiao, and F. Yuan, Phys. Lett. B**763**, 208 (2016) [arXiv:1604.04250].
- [9] L. Adamczyk *et al.* [STAR Collaboration], Phys.Rev. C**96**, 024905 (2017) [arXiv:1702.01108].
- [10] J. Norman [for ALICE Collaboration], arXiv:1901.02706.
- [11] J. Norman [for ALICE Collaboration], talk at Hard Probes 2020; <https://indico.cern.ch/event/751767/overview>; arXiv:2009.08261.
- [12] M. Gyulassy, P. Levai, J. Liao, S. Shi, F. Yuan, and X.N. Wang, Nucl. Phys. A**982**, 627 (2019) [arXiv:1808.03238].
- [13] P. Jacobs, private communication.
- [14] B. Wu, JHEP **1110**, 029 (2011) [arXiv:1102.0388].
- [15] T. Liou, A.H. Mueller, and B. Wu, Nucl. Phys. A**916**, 102 (2013) [arXiv:1304.7677].
- [16] J.-P. Blaizot and Y. Mehtar-Tani, Nucl. Phys. A**929**, 202 (2014) [arXiv:1403.2323].
- [17] B.G. Zakharov, JETP Lett. **70**, 176 (1999) [hep-ph/9906536].
- [18] R. Baier, D. Schiff, and B.G. Zakharov, Ann. Rev. Nucl. Part. Sci. **50**, 37 (2000) [hep-ph/0002198].
- [19] B.G. Zakharov, JETP Lett. **108**, 508 (2018) [arXiv:1807.09742].
- [20] B.G. Zakharov, JETP **129**, 521 (2019) [arXiv:1912.04875].
- [21] E. Iancu, P. Taels, and B. Wu, Phys. Lett. B**786**, 288 (2018) [arXiv:1806.07177].
- [22] J.D. Bjorken, Phys. Rev. D**27**, 140 (1983).
- [23] R. Baier, Nucl. Phys. A**715**, 209 (2003) [hep-ph/0209038].
- [24] R. Baier, Yu.L. Dokshitzer, A.H. Mueller, and D. Schiff, Phys. Rev. C**58**, 1706 (1998) [hep-ph/9803473].
- [25] C.A. Salgado and U.A. Wiedemann, Phys. Rev. Lett. **89**, 092303 (2002) [hep-ph/0204221].
- [26] N.N. Nikolaev and B.G. Zakharov, Z. Phys. C**64**, 631 (1994) [hep-ph/9306230].
- [27] K.M. Burke *et al.* [JET Collaboration] Phys. Rev. C**90**, 014909 (2014) [arXiv:1312.5003].
- [28] B.G. Zakharov, Phys. Atom. Nucl. **61**, 838 (1998) [hep-ph/9807540].
- [29] N.N. Nikolaev and B.G. Zakharov, Phys. Lett. B**332**, 184 (1994) [hep-ph/9403243].
- [30] B.G. Zakharov, JETP Lett. **88**, 781 (2008) [arXiv:0811.0445].
- [31] P. Lévai and U. Heinz, Phys. Rev. C**57**, 1879 (1998) [hep-ph/9710463].
- [32] B.G. Zakharov, J. Phys. G**40**, 085003 (2013) [arXiv:1304.5742].
- [33] B.G. Zakharov, J. Phys. G**41**, 075008 (2014) [arXiv:1311.1159].
- [34] O. Kaczmarek and F. Zantow, Phys. Rev. D**71**, 114510 (2005) [hep-lat/0503017].
- [35] B.Z. Kopeliovich and B.G. Zakharov, Phys. Rev. D**44**, 3466 (1991).
- [36] N.N. Nikolaev and B.G. Zakharov, Phys. Lett. B**327**, 149 (1994) [hep-ph/9402209].
- [37] Yu.L. Dokshitzer, V.A. Khoze, and S.I. Troyan, Phys. Rev. D**53**, 89 (1996) [hep-ph/9506425].
- [38] B.G. Zakharov, JETP **128**, 243 (2019) [arXiv:1806.04723].